JACS
JOURNAL OF THE AMERICAN CHEMICAL SOCIETY
Article
pubs.acs.org/JACS

Modulating the Electron–Hole Interaction in a Hybrid Lead Halide Perovskite with an Electric Field

Tomas Leijtens,[†,‡] Ajay Ram Srimath Kandada,[*,†] Giles E. Eperon,[‡] Giulia Grancini,[†] Valerio D'Innocenzo,[†,§] James M. Ball,[†] Samuel D. Stranks,[‡] Henry J. Snaith,[‡] and Annamaria Petrozza[*,†]

[†]Center for Nano Science and Technology@Polimi, Istituto Italiano di Tecnologia, via Giovanni Pascoli 70/3, 20133 Milan, Italy
[‡]Clarendon Laboratory, University of Oxford, Parks Road, Oxford OX1 3PU, United Kingdom
[§]Dipartimento di Fisica, Politecnico di Milano, Piazza L. da Vinci, 32, 20133 Milan, Italy

Supporting Information

ABSTRACT: Despite rapid developments in both photovoltaic and light-emitting device performance, the understanding of the optoelectronic properties of hybrid lead halide perovskites is still incomplete. In particular, the polarizability of the material, the presence of molecular dipoles, and their influence on the dynamics of the photoexcitations remain an open issue to be clarified. Here, we investigate the effect of an applied external electric field on the photoexcited species of $CH_3NH_3PbI_3$ thin films, both at room temperature and at low temperature, by monitoring the photoluminescence (PL) yield and PL decays. At room temperature we find evidence for electric-field-induced reduction of radiative bimolecular carrier recombination together with motion of charged defects that affects the nonradiative decay rate of the photoexcited species. At low temperature (190 K), we observe a field-induced enhancement of radiative free carrier recombination rates that lasts even after the removal of the field. We assign this to field-induced alignment of the molecular dipoles, which reduces the vibrational freedom of the lattice and the associated local screening and hence results in a stronger electron–hole interaction.

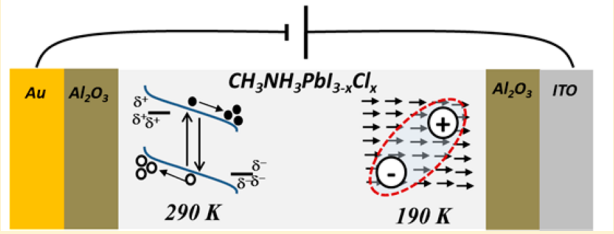

INTRODUCTION

Hybrid lead halide perovskites offer a unique set of properties that makes them ideally suited for optoelectronic applications.[1−3] They are solution processable and have tunable bandgaps, long carrier diffusion lengths, and high photoluminescence yields.[4,5] These properties have allowed photovoltaic devices comprising $CH_3NH_3PbI_3$ to reach over 20% efficiency after just a few years of research,[6,7] have enabled the realization of efficient and tunable light-emitting diodes (LEDs),[8] and allow the materials to be capable of lasing.[9−11] Their ability to self-assemble with low crystallization energies makes them on one hand extremely versatile but on the other hand makes them intrinsically complex; the presence of various types of interactions and structural disorder may play an important role in the optoelectronic properties. However, so far, the difficulty in predicting the response of these materials to external stimuli makes it challenging to understand them via frameworks corresponding to previously defined technologies.

Quoted values for the exciton binding energy in $CH_3NH_3PbI_3$ have varied from 2 to 50 meV,[12−16] and the consensus is that the predominant species at room temperature and solar fluences are free carriers.[9,12,17] Photoluminescence studies have also demonstrated that the photoexcitations have long lifetimes of over 100 ns with photoluminescence quantum yields (PLQY) of the order of 10–20%.[9,18] Theoretical work proposed that the long lifetimes and low exciton binding energies could be due to separation of electrons and holes to local energetic minima and maxima at ferroelectric domain walls.[19−21] Other recent works suggests that the rotational freedom of the molecular dipoles can affect the effective dielectric constant of the perovskite at frequencies relevant (THz) to electronic interactions, thus influencing electron–hole interactions.[20,22] The influence of the molecular dipole on the dielectric response of the material becomes especially relevant considering that the predominant photoexcitation, at room temperature, is a correlated electron–hole plasma whose interaction strength will depend on the dielectric constant of the material at the relevant frequency.[16]

Another subject of debate has been to do with the long-lived polarization of the perovskite under applied electric fields.[23−25] This effect manifests itself as a large hysteresis in the measured current–voltage curves of perovskite solar cells and LEDs in planar heterojunciton architectures, depending on the contact materials used.[8,23,26−29] The community has been working to understand whether the observed polarization is due to the migration of mobile charged defects, molecular dipole alignment, or a ferroelectric response. Most of the recent work supports the hypothesis that ion migration[23,27,30] should dominate any ferroelectric behavior at room temperature.[31]

Received: August 27, 2015
Published: November 18, 2015

DOI: 10.1021/jacs.5b09085
J. Am. Chem. Soc. 2015, 137, 15451−15459

In order to gain further understanding of the interplay between the different constituents of this complex hybrid structure in a functional architecture, we address here the effect of an external electric field on the photophysics of $CH_3NH_3PbI_3$ thin films. These investigations will not only shed light on the peculiar response that the material has demonstrated in working devices such as solar cells and LEDs where the polarization of the thin film is unavoidable,[8,26,27] they will also allow us to tackle a fundamental issue which regards the role of the organic dipole in determining the nature and the fate of the photoexcitations.

We study both the steady-state and the time-resolved photoluminescence (PL) response as a function of an electric field by sandwiching the perovskite thin film between two noninjecting contacts. PL, representative of the population of excited species, is an ideal process to define and monitor different possible decay pathways such as free carrier recombination, geminate exciton recombination, and charge trapping.[32] Recent and independent works have demonstrated that the PL decay in $CH_3NH_3PbI_3$ thin films can be described by a radiative nongeminate electron−hole recombination process and nonradiative relaxation pathways. The temporal evolution of the excited carrier population n can be modeled by considering a bimolecular intrinsic radiative recombination coefficient, B_{rad}, and a nonradiative monomolecular trapping rate (A), i.e., $dn/dt = -An - B_{rad}n^2$.[18,33] The dynamics are dictated by the trapping rate at low excitation densities, and after the traps are completely filled, the intrinsic bimolecular rate is revealed.[9,18] An increase in bimolecular recombination rate will result in an increased PL yield, while an increase in the monomolecular decay rate will result in a decrease in PL yield.

Within this framework, at room temperature (RT) we find that an applied electric field instantaneously quenches the photoluminescence, as expected from field-induced carrier separation and drift.[34−36] However, over a long time scale we also find a significant reduction in the nonradiative monomolecular decay rate. The latter suggests that mobile defects, which can drift under application of an electric field,[23] are at least in part responsible for the nonradiative decay pathway. We also performed the same experiment at 190 K in order to reduce the influence of temperature activated processes. We find that the radiative decay rate is enhanced upon electric field application, and we even observe evidence for rapid geminate recombination. The result is an increase in relative PLQY by up to 10% after applying a field of approximately 150 kV cm^{-1}. Combining these findings with electric field dependent Raman spectroscopy, we propose that the electric field induces an alignment and "locking" of the organic dipoles which enhances the electron−hole interaction. This is only observed at lower temperatures where thermal disorder makes it difficult to align the dipoles with the relatively low electric fields used here. The results emphasize the importance of the nature and orientational freedom of the A cation in determining electron−hole interactions.

RESULTS AND DISCUSSION

To probe the effect of an electric field on the excited state dynamics in $CH_3NH_3PbI_3$ films, we prepared samples with noninjecting contacts in a capacitor configuration, as depicted in Figure 1a. Here, the noninjecting layers are made of 100 nm of Al_2O_3, deposited via atomic layer deposition (ALD). The perovskite was deposited on top of the bottom Al_2O_3 layer via single step spin-coating of $PbCl_2$ and methylammonium iodide

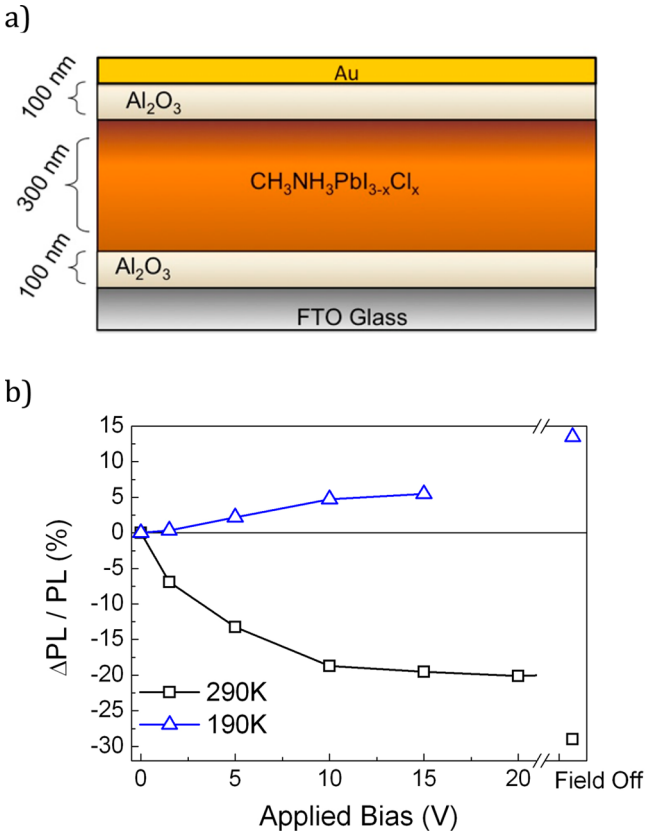

Figure 1. (a) Schematic structure of the device architecture used throughout this study. (b) Change in photoluminescence given as a percentage change as a function of applied electrical bias at room temperature (black squares) and 190 K (blue triangles). The PL intensity was monitored at the respective peaks of 775 and 790 nm for RT and 190 K. The excitation was provided by a 510 nm excitation at 3 $\mu J\ cm^{-2}$ and a 10 MHz repetition rate. The samples were kept under vacuum during the measurements.

precursors,[2] and the top Al_2O_3 layer was deposited on top of the perovskite via ALD. The samples did not undergo any major degradation during processing, as indicated by the absorption and PL spectra presented in Figure S1.

Figure 1b depicts the change in steady state PL intensity as a function of applied bias at RT and at 190 K. Any changes to the steady state PL intensity correspond directly to changes in relative PL quantum yield (PLQY). We note that the application of the electric field did not result in any evident changes to the absorption of the samples and only minor changes in PL peak position (Figure S2). We observe strikingly different behaviors when we work at the two different temperatures. At RT the field induces a reduction in the PLQY, while at low temperature an enhancement of the relative PLQY by up to 10% is observed. Moreover, we note that in both the cases the field-induced effects persist and even increase when the external field is removed as shown in Figure 1b. Qualitatively, this observation suggests that there are several processes that are responding to the applied electric field with different temperature dependencies. We present the behavior at several additional temperatures in Figure S3 to demonstrate that the two effects are in competition at intermediate temperatures. In order to understand these processes, we performed time-resolved PL measurements under an applied electric field.

DOI: 10.1021/jacs.5b09085
J. Am. Chem. Soc. 2015, 137, 15451−15459

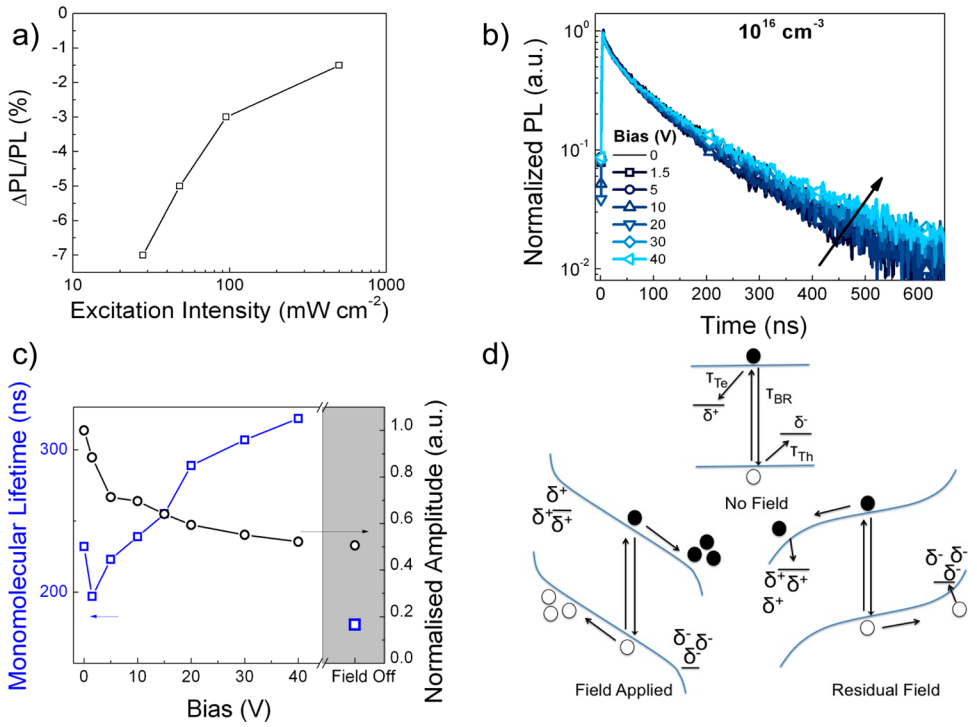

Figure 2. (a) PL quenching at RT and 3 V applied under continuous wave excitation at 630 nm. (b) Photoluminescence decay at various applied biases at room temperature and an excitation density of 10^{16} cm^{-3}. The arrows are to aid the eye. The decays are measured under an excitation density of 10^{16} cm^{-3}. (c) Monomolecular decay lifetimes extracted from single-exponential fits to the last 5% of the decays in to quantify the charge trapping kinetics. The normalized initial (t = 0) amplitudes are plotted on the right axis. (d) Schematic depiction of the decay pathways before, during, and after the application of the electric field, where charged defects are represented as partial positive or negative charges (we include both electron and hole traps because we cannot distinguish between them) and can migrate in response to an electric field. An excitation wavelength of 510 nm was used at a 1 MHz repetition rate, and the PL was collected at its peak of 775 nm.

First, we will discuss the influence of the applied electric field at RT, bearing in mind that the PL dynamics are dictated by an intrinsic bimolecular radiative recombination mechanism once trap states are completely filled at high fluences. Quenching of the PL by an applied electric field as observed here (Figure 1b) is commonly observed in both fully inorganic and organic semiconductors and can be associated with a simple mechanism:[34−36] photogenerated electrons and holes drift to opposite sides of the device, reducing the probability of their radiative recombination. To confirm that this is the predominant effect of the applied field at room temperature, we have measured the relative PL quenching (ΔPL/PL) as a function of the excitation fluence at a fixed applied voltage (Figure 2a). As the fluence is increased, the PL quenching is reduced, in agreement with the fact that the generated carriers drift toward the electrodes, thus screening the applied field and reducing the effect of the applied field. Note that the charge required to screen the applied bias matches well with predicted carrier densities at the different excitation fluencies (see discussion in Note 2 of the Supporting Information), which is further evidence of charge carrier accumulation at the noninjecting contacts. The PL dynamics measured at a high excitation density of 10^{17} cm^{-3} (bimolecular regime[18,37]), recorded in a time scale of hundreds of nanoseconds, show, in agreement, a reduction of the PL intensity at t = 0 and slight elongation of bimolecular recombination dynamics as the applied voltage is increased (see Figure S4 in the Supporting Information).

In addition to this dominant phenomenon, we have also noticed a concomitant mechanism. In Figure 2b we show the PL decays generated at an excitation density of 10^{16} cm^{-3}. In particular, we look at the last 5% of the PL signal decay, when the density of photogenerated carriers should not be larger than 5×10^{14} cm^{-3} which is substantially below the 10^{15}−10^{16} cm^{-3} trap density reported for $CH_3NH_3PbI_3$ films prepared in this way.[18,33] We observe that the decays become monoexponential (linear on the log[PL] vs time scale), and by plotting the lifetimes as a function of applied electric field (Figure 2c), we observe a very strong reduction in decay rate (i.e., longer monomolecular lifetime). It is worth recalling that as the photocarrier density becomes smaller and smaller (i.e., on longer time scales after photoexcitation when looking at the PL dynamics or by simply exciting at lower excitation fluencies), the PL dynamics start falling in the charge trapping regime.[18,32,33] Thus, in such framework, the slower monomolecular lifetimes represent a reduction in the trapping rate and thus a reduction in the trapping probability in addition to the reduction of carrier recombination (seen as the reduced (t = 0) PL intensity, Figure 2c).

Surprisingly, however, once the electric field is removed, the monomolecular lifetime becomes even shorter than before the sample had been exposed to a field, and the PL yield is even further reduced (Figure 2c). This effect is long-lasting, with the PL remaining quenched for over tens of seconds after the field is removed (see Figure S5). Thus, while the electric field actually slows the nonradiative monomolecular recombination during application, it induces a longer-lasting change in the film that increases the nonradiative monomolecular trapping rate after removal of the electric field.

DOI: 10.1021/jacs.5b09085
J. Am. Chem. Soc. 2015, 137, 15451−15459

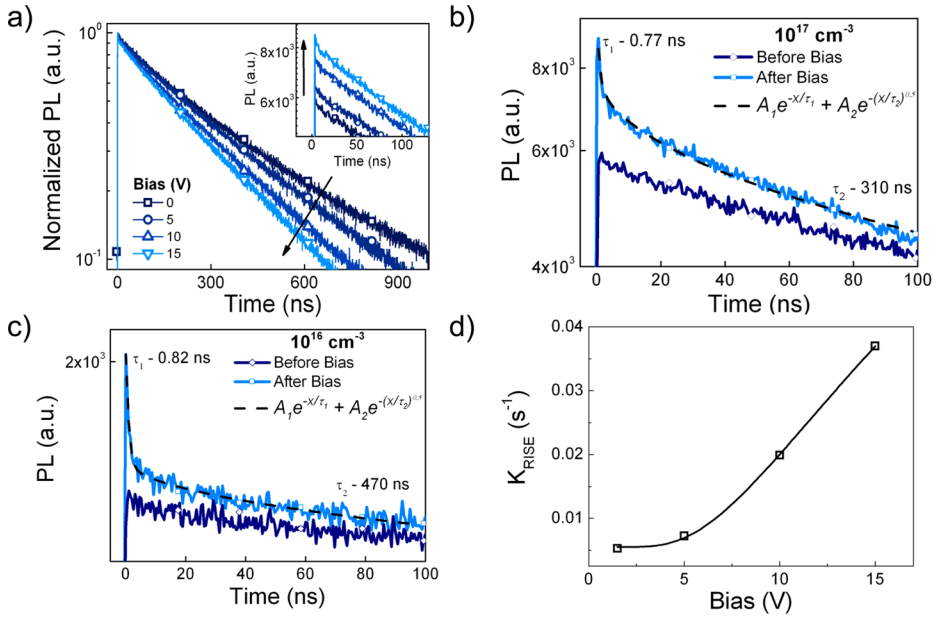

Figure 3. (a) Photoluminescence decays a function of applied bias performed at 190 K. The excitation density is 10^{17} cm^{-3}. (b) Photoluminescence decays before and after the application of an electric field, demonstrating the long-lasting change to the perovskite material persisting after the field is removed. The excitation density is 10^{17} cm^{-3} at a wavelength of 510 nm. (c) The same as (b) but at an excitation density 10^{16} cm^{-3}. The time constants are the lifetimes extrapolated from fits to the decay using a monoexponential decay coupled with a stretched exponential using 0.5 as the stretch factor. (d) Rate constant of the slow increase in relative PLQY upon application of different biases is plotted as a function of bias. The solid line is a fit to an Arrhenius rate law, demonstrating that the process is likely to be one involving an activation energy, as discussed in the main text. An excitation wavelength of 510 nm was used at a 1 MHz repetition rate, and the PL was collected at its peak of 790 nm.

Long-lasting polarization has been often observed in this material and has been correlated to charged ion migration.[23,27,38] We propose that here the electric field induces the defect sites to migrate to opposite ends of the device just as the carriers do, decreasing the monomolecular decay rate by clearing the defects from the bulk. This mechanism can be confirmed by applying a field at a high excitation density, where photogenerated charge screening prevents a significant reduction in bimolecular decay (as shown in Figure 2a), and the high density of charge results in fast bimolecular recombination that competes with field-induced drift. Here, the dominant effect should be a slight increase in PL efficiency as charged defects drift slowly out from the bulk together with carriers of the same charge. The data are plotted in Figure S8a and do in fact demonstrate a slight increase in PL yield which grows over the first 10 s, consistent with the time scale of ion migration reported for this material.[23,26,39] Once the electric field is removed, the accumulated ions at the contacts polarize the device in the opposite direction to that in which the field was applied. Photogenerated carriers will drift in response to this remnant field toward defects of the opposite charge where they will be trapped and recombine nonradiatively.

We also performed the same measurement on a sample with a very high monomolecular decay rate (i.e., high trap density) to observe the effect of applying an electric field. We plot the results in Figure S6 and demonstrate an even more pronounced reduction in decay rate with applied electric fields, consistent with our hypothesis that mobile charged defects are in part responsible for the monomolecular decay in perovskite films. We also note that we measured the decays at both positive and negative biases to confirm that the device is indeed symmetric; results are plotted in Figure S7.

To summarize the effects of an applied electric field on the carrier dynamics at RT, we draw a scheme (Figure 2d) to qualitatively depict the photophysics in the perovskite before, during, and after the application of an electric field at room temperature. Before the application of the electric field, free carriers can decay either via bimolecular recombination or via a monomolecular trapping process.[18,33] We do not distinguish between electron or hole traps and so draw both pathways. Upon application of an electric field, free carriers and charged defects migrate toward the contacts, reducing both bimolecular and monomolecular recombination rates. Upon removal of the electric field, the film remains temporarily polarized because charged defects have accumulated at opposite ends of the film. This means that the probability and rate of bimolecular decay remain slowed and that free carriers now drift toward defects of the opposite charge, resulting in more rapid monomolecular decay and an overall further PL quenching. The results are highly consistent with our hypothesis that charged defects are at least partly responsible for the monomolecular charge trapping pathway and that these defects can migrate in response to an electric field, polarizing the material.[23−26,28,29] The residual polarization and its influence on the PL in the material are also consistent with recent observations of transient changes to the external quantum efficiency of perovskite LEDs,[8] indicating that the defect distribution and associated electric fields are influential upon perovskite LED operation at room temperature.

Two main field-induced effects can be identified by the PL dynamics of $MAPbI_3$ at room temperature: (1) reduction of the intrinsic radiative recombination yield as a direct consequence of photogenerated carrier drift (Figure 2a); (2) reduction of the carrier trapping upon ion migration which is eventually identified as being due to migration of mobile defects. It is worth while to underline that though, here, we can safely correlate the charge trapping process to the presence of charged defects, the change induced on the electronic landscape of the

DOI: 10.1021/jacs.5b09085
J. Am. Chem. Soc. 2015, 137, 15451−15459

semiconductor by the ion displacement still remains a topic to be investigated. There is also the possibility that the ionic species that moves in response to the electric field is a vacancy−interstitial pair created by the application of the electric field. We cannot easily distinguish between the motion of pre-existing defects and those that may be created during the experiment. However, the samples exhibit absolutely no signs of degradation after application of the bias (Figure S2), and recent published results have also demonstrated the ion motion to be primarily reversible and not lead to any permanent degradation even over 500−1000 h of device operation.[40−41] We also note that our investigations were focused on phenomena occurring in a time window up to tens of seconds; thus, we do not exclude the possibility of other structural changes occurring over far slower time scales (i.e., tens of minutes; see Figure S8b,c) as recently pointed out by Gottesman et al.[42]

When we cool the sample to 190 K (above the tetragonal to orthorhombic phase transition), we observe very different behavior: here the PL is enhanced by the electric field (Figure 1b). The photophysical processes at low temperature are likely to differ from those at room temperature. It has been already shown that in such experimental conditions the PLQY can approach 100% at high excitation density, the trapping rate is reduced, ions are less mobile, and the material may begin to show evidence of excitonic behavior.[12,18,22]

We present time-resolved PL decays at 190 K as a function of applied bias and at an excitation density of 10^{17} cm^{-3} in Figure 3a. As the field is increased, we see an enhancement of the initial amplitude and a reduction in the radiative lifetime (1/e) to 80% of the initial value (see Figure S9 for detailed fitting results). As stated above, at the given experimental conditions, i.e., low temperature and a relatively high excitation density, we are predominantly exploring the effect of the applied bias on radiative bimolecular recombination of carriers.[18,33] Our observations suggest that the application of the electric field has mainly increased the probability and rate of radiative decay which seems to overcome the drift-induced quenching.

Importantly, the PL is even further enhanced after the electric field has been removed (Figure 1b and Figure S10), indicating that a long-lived change has occurred in the material that has a beneficial influence on the radiative decay rate. In Figure 3b,c we present time-resolved PL decays before and after application of the electric field for 10^{17} and 10^{16} cm^{-3} excitation densities, respectively. We now observe the appearance of a very high intensity and rapid emission with a lifetime of less than 1 ns along with the usual radiative bimolecular decay over hundreds of nanoseconds. We fit the decays by considering monomolecular and bimolecular rates in the form of a monoexponential decay coupled with a stretched exponential (stretch factor 0.5) decay. From the fits, we find that the subnanosecond decay rate ($\tau \sim 800$ ps) is unaffected by a 10-fold reduction in excitation density, while the lifetime of the slow component is reduced. This is all consistent with the idea that the slow component is dictated by bimolecular recombination, while the fast component is related to a monomolecular process that we assign to recombination of geminate pairs. Shortening of bimolecular lifetimes with the appearance of a geminate subnanosecond component suggests a field-induced enhancement of the electron−hole coulomb interaction that remains even after the removal of the field.

Though the predominant route of radiative emission in these materials was proposed to be via bimolecular recombination of free carriers,[37] a role of the coulomb correlation between the electrons and holes was also suggested,[16] and the carriers were also proposed to be polaronic in nature.[43,44] Here, immediately after the photoexcitation, due to the field-induced enhancement of the interaction, electrons and holes undergo geminate recombination, resulting in the efficient subnanosecond PL. In later times, whichever carriers did not geminately recombine dominate the decay via the previously discussed radiative bimolecular behavior. However, because of the enhanced coulomb interactions, the radiative bimolecular rate is faster. We observe the subnanosecond component only when the field is removed because in the presence of the field the geminate pairs can be dissociated and the carriers can drift away from each other, reducing the probability of their geminate recombination.[17,18,33]

We also note that these low-temperature changes to the PL happen at an extremely slow rate and are long-lasting (seconds to minutes time scales, see Figure S10). We extract the rate constant of the CW-PL growth upon application of the electric field in Figure 3d and demonstrate that it has an Arrhenius-like dependence on the applied bias, just like the absolute ΔPL/PL shown in Figure 1b. This activation energy would be calculated as 23 V across the device, which corresponds to approximately 20 meV per unit cell (see Note 1 in Supporting Information), but because the effective rate may be dependent on the relative rates of forward and backward reactions (as discussed later), this number is merely an approximation of the rough magnitude of energy required for the observed field-induced changes. These observations suggest that we are perceiving an effect with an activation energy provided by the application of an electric field.

One of the unique characteristics of the hybrid perovskites is the presence of the organic cation. This cation has a permanent dipole moment within the lattice with a certain degree of rotational freedom. It can be hypothesized that the external bias can align the dipoles in the direction of the field. Ferroelectric and antiferroelectric ordering due to molecular dipole alignment has indeed been theoretically proposed in these materials, especially at low temperatures.[20,21,31] Such a process has to compete with thermally activated processes such as the free rotation of the cation that will disrupt the ferroelectric ordering. Hence, to obtain a net dipole alignment, energy in excess of the available thermal energy would have to be supplied to overcome the thermal "disordering". This is why the PL enhancement is only observed at low temperatures where thermal energy cannot dominate the potential gradient provided by the applied field. We also point out that this means that a similar phenomenon due to cation rotation is unlikely to play a role in the hysteresis often observed in current−voltage curves of this material.

Insights into possible field-induced structural changes can be given by Raman spectra of perovskites under the applied bias that we present in Figure 4. Raman spectroscopy probes the vibrational modes of the material and hence the interaction between the organic and inorganic moieties.[45,46]

As reported in Figure 4, we observe substantial changes in the Raman spectrum when an electric field is applied. Previous work has distinguished three main spectral regions in the $MAPbI_3$ Raman spectrum. One, between 50 and 70 cm^{-1}, carries information on the vibrational modes of the pure inorganic network; the other, between 105 and 120 cm^{-1}, is a convolution of the vibrational modes of the inorganic network associated with the libration of the organic cation; finally, the

DOI: 10.1021/jacs.5b09085
J. Am. Chem. Soc. 2015, 137, 15451−15459

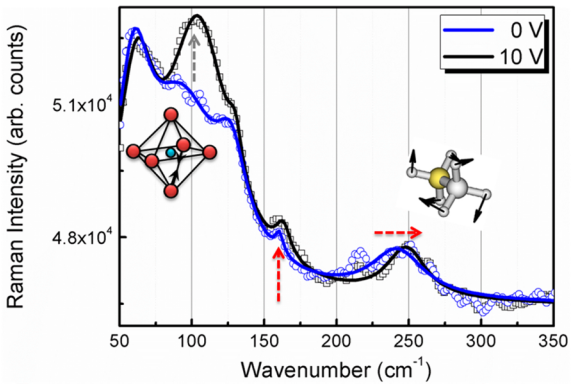

Figure 4. Raman spectra collected at 0 V (blue open circles) and at 10 V (black open squares) bias applied across the perovskite film. The solid lines represent the fit as a sum of five peaks (see table in Figure S11 for fit details).

region above 120 cm^{-1} is mainly dominated by the libration (150 cm^{-1}) and torsional (250 cm^{-1}) modes of the organic cation within the inorganic network.[45−47] The $MAPbI_3$ structure is a fluctuating structure where orientational disorder, characteristic of the interaction between the organic dipole and the inorganic cage, can be modulated by external agents. In the presence of electric field we clearly observe a shift and narrowing of the transitions related to the organic modes, behavior theoretically predicted when the degree of freedom of the cation is reduced.[45,47,48] These results are consistent with the idea that the field reduces the orientational mobility of the organic cation, thus limiting the degrees of freedom of the vibrational modes in the perovskite lattice. Of course, this phenomenon will be more and more effective and easier to disentangle when we reduce the available thermal energy, as recently suggested by Miyata et al.[15] and Grancini et al.[22]

The rotation of $CH_3NH_3^+$ molecular dipoles has been previously predicted to have an activation energy of around 50 meV per unit cell,[19] not so different from our approximated effective activation energy of 20 meV per unit cell. However, it is also expected to occur extremely rapidly (picoseconds time scale),[49] while we observe the overall changes (from a structural and optical point of view) in a longer time window. The applied bias per unit cell in our experiments is around 150 kV cm^{-2} or 15 meV per unit cell at most (see Note 1 in the Supporting Information), which is still close to thermal energy at 190 K that is trying to disrupt the alignment. Therefore, the slow changes we observe here is an outcome of an equilibration process needed to achieve a large density of "aligned" domains that are not disrupted by thermal fluctuations and point defects,[22] which can then result in a macroscopically observable effect.[20]

Thus far, we have shown evidence that the application of an electric field can cause slow structural rearrangement of the material which seems to correlate eventually with an enhanced electron−hole coulomb interaction to such an extent that we can even observe rapid geminate recombination phenomena. Alignment of dipoles induces dipole twinning and restricts their rotations.[22] This will reduce the effective dielectric permittivity of the material at frequencies (GHz−THz) which are relevant for carrier interaction.[15,20,22,49,50] Recently, we have demonstrated that the relative degree of freedom of the organic cation controlled by tuning the polycrystallinity of the sample can strongly influence the electron−hole interactions;[22] here the scenario is similar, albeit the control is achieved by the applied electric field. Charge carriers in $CH_3NH_3PbI_3$ have been suggested to have polaronic character.[43,44] As a result, the probability of bimolecular recombination will be affected by their mobility and the coulomb interaction between them, wherein the rate is inversely proportional to the dielectric constant. As the dielectric permittivity is lowered due to electric-field-induced dipole alignment and structural ordering, the coulomb capture radius of carriers increases, thus resulting in a higher radiative rate.

Following the proposed mechanisms, involving alignment of the molecular dipole, we schematically present the proposed photophysical picture before, during, and after application of the electric field at low temperatures in Figure 5. Before the

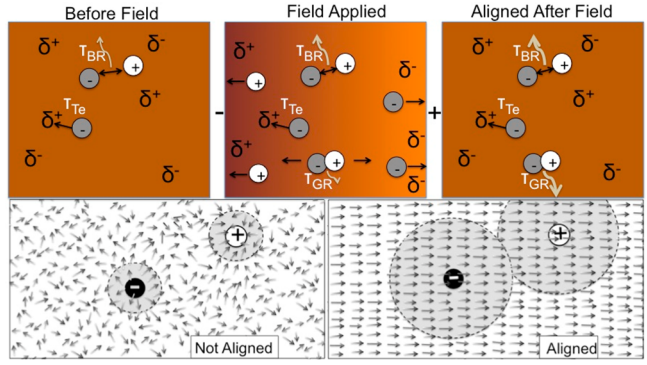

Figure 5. Schematic description of the behavior of photogenerated species before, during, and after the application of an electric field. The different decay processes of trapping (T_{Te}), bimolecular recombination (T_{BR}), and geminate exciton recombination (T_{GR}) are depicted. At RT, both free carriers and defects migrate in response to the electric field to slow radiative and nonradiative decay, respectively. At low temperature, trap-related processes play a minor role, but bimolecular and geminate recombination pathways are enhanced after the application of the electric field. Hole trapping is ignored for the sake of simplicity, but the picture would not change if it were holes that were trapped rather than electrons. The bottom right panel displays the proposed role of the molecular dipole before and after alignment, focusing on the role of coulomb screening: dipole alignment effectively reduces coulomb screening and enlarges the carrier capture radius to enhance geminate recombination.

application of the field, the decay pathway is predominantly bimolecular recombination of free carriers with a small contribution of monomolecular trapping processes (at the high fluence of 10^{16}−10^{17} cm^{-3}).[17,18,33] Upon application of the electric field, the dipoles become aligned and coulomb interactions are enhanced. The result is an enhanced bimolecular decay which competes with the drift of carriers in response to the electric field. After the electric field is removed, the dipoles stay aligned and the electron−hole interactions remain strong so that we observe evidence for geminate recombination and largely enhanced bimolecular decay rates. The schematics in the fourth panel describe how alignment of the dipoles may counter dielectric screening to enlarge the carrier capture radius and thus enhance both geminate recombination and bimolecular recombination rates.

Some might argue that a net alignment of dipoles across the full film would induce a net field through the device where the dipole potential is assumed to sum across the film. However, we point out that Rappe et al. have demonstrated that completely aligned dipoles do not create a long-range electric field,[21] while

DOI: 10.1021/jacs.5b09085
J. Am. Chem. Soc. 2015, 137, 15451−15459

the potential across poled ferroelectric thin films is constant with thickness (i.e., the field decreases with thicker films),[51−53] indicating that alignment of dipoles will not create a net electric field across the perovskite films, and the only effective change is the change in the dielectric environment associated with a reduction in cation orientational freedom.

The proposed mechanisms for the low-temperature PL enhancements have large implications for our understanding of organic−inorganic metal halide perovksite semiconductors. The fact that the locking of the dipoles has such a large influence on the material's photophysical properties is an indication that the dipoles, and their influence on the crystal lattice characteristics, play a crucial role in allowing this class of material to achieve such weak electron−hole interaction and long carrier lifetimes. Tuning this polarizability by using cations (such as Cs) with different dipole moments and freedom to rotate will provide an interesting avenue for future work.

CONCLUSIONS

By monitoring the photoluminescent properties of $CH_3NH_3PbI_3$ perovskite films under different electric fields and temperatures, we can elucidate some of the working principles of the semiconductor. We find that the electric field causes long-lasting changes in the material properties. At RT, along with instantaneous PL quenching due to carriers drift, we observe field-induced defect migration, which polarizes the films and reduces the PL monomolecular decay rate which is associated with nonradiative trapping phenomena. First of all, this suggests that the presence of mobile ions in the film represents a possible source for detrimental recombination channels. Then, the fact that field-induced ion migration to the electrodes improves the optoelectronic property of the semiconductor (i.e., the trapping rate reduces) seems to indicate that the ionic crystal is intrinsically stable at room temperature under an applied electric field and that the mobile ions are simply the residue of an incomplete stoichiometric synthesis.

At lower temperatures, however, field-induced dipole alignment and structural ordering seem to dominate. We find that this enhances electron−hole interaction and increases the radiative decay rates. The latter observations are rationalized by the fact that locking the molecular dipoles will reduce their rotational degrees of freedom and hence the effective dielectric constant to enhance electron−hole interactions, manifested in increased geminate and bimolecular recombination rates. These findings shed light on the crucial role of the molecular dipole on the weak electron−hole coulomb interaction and slow bimolecular recombination that have been proven essential to the efficient functioning of these materials in photovoltaic devices. Moreover, they also provide interesting guidelines for an educated design of materials: selective control of the organic−inorganic moieties interactions can help tuning the electron−hole interaction and their photophysical dynamics according to the desired functionality.

EXPERIMENTAL METHODS

Sample Preparation. CH_3NH_3I was prepared by reacting methylamine, 33 wt % in ethanol (Sigma-Aldrich), with hydroiodic acid (HI), 57 wt % in water (Sigma-Aldrich), at room temperature. HI was added dropwise while stirring. Upon drying at 100 °C, a white powder was formed, which was dried overnight in a vacuum oven and recrystallized from ethanol before use.

Patterned fluorine-doped tin oxide (FTO) substrates were coated with 100 nm of compact Al_2O_3 with a home-built atomic layer deposition (ALD) setup, using high-purity trimethylaluminum and water precursors. Nitrogen was used as carrier and purging gas, with the flow rate set to 20 sccm and controlled by a mass flow controller. The deposition was carried out at 102 °C, base pressure of 0.3 mbar, and growth rate of 1.07 Å per cycle. Each cycle consisted of 5 s of precursor dose and 20 s of purging, with trimethylaluminum dosed first, followed by water.

After a 5 min oxygen plasma clean, 300 nm perovskite films were spin-coated (2000 rpm) on top from a 40 wt % solution of $PbCl_2$ and CH_3NH_3I (1:3 molar ratio) in dimethylformamide (DMF) in a nitrogen-filled glovebox. Here, the wet films were allowed to dry for 30 min at room temperature, after which they were annealed at 90 °C for 90 min, and finally at 100 °C for another 30 min. Another 100 nm layer of Al_2O_3 was then deposited on top of the perovskite layer via ALD. As shown in the Supporting Information, the final films showed no sign of degradation. Semitransparent (25 nm) gold electrodes were then deposited via thermal evaporation through a shadow mask.

Photoluminescence Measurements. The samples were mounted in a cryostat and held under vacuum during measurement. The steady state photoluminescence (PL) quenching or enhancement was measured by monitoring the peak of the PL with 5 nm bandwidth over time and as a function of applied bias. The PL was allowed to stabilize for over 5 min for each applied bias. The samples were oriented such that the excitation and PL detection were from the transparent FTO side.

Time-resolved PL measurements were taken after the steady state PL had stabilized and were taken with 128 ps resolution at the PL peak with 5 nm bandwidth. These PL measurements were all taken using a commercial time correlated single photon counting (TCSPC) setup (FluoTime 300, PicoQuant GmbH), and the samples were excited by a pulsed laser head (LDH-P-C-510, PicoQuant GmbH) at 507 nm at varying repetition rates (1 MHz for time-resolved decays and 10 MHz for steady state measurements).

Time-resolved fluorescence measurements were also performed using a femtosecond laser source and either a streak camera detection system (Hamamatsu C5680). An unamplified Ti:sapphire laser (Coherent Chameleon Ultra II) operating at 80 MHz was tuned to provide pulses with central wavelengths of 960 nm, energies of ∼50 nJ, and temporal and spectral bandwidths of ∼140 fs and ∼5 nm, respectively. The pulses were then focused onto a BBO crystal, and the second harmonic generated (at 480 nm) was employed to photoexcite the sample. The emitted fluorescence radiation was collected, filtered with a long pass filter cutting at 750 nm in order to remove the excitation scattering, and subsequently focused on a spectrometer coupled to the detection system. The measurements were performed using a linear voltage sweep module at either 1 or 2 MHz repetition rate excitation, achieved through the use of an acousto-optical modulating pulse picker (APE Pulse Select).

Absorption Measurements. The transmission spectra of the samples at different applied biases were taken in a cryostat under vacuum using a tungsten probe light focused on the sample. The transmitted probe light is passed through a monochromator and then detected by a photodiode. The baseline was taken for the transmission through the full setup (including cryostat) without any sample. The optical density was then then taken as $OD = -\log(T_1/T_0)$, where T_1 and T_0 correspond to the light transmitted through the sample and the cryostat windows, respectively.

Raman Spectroscopy. The micro-Raman system is based on an optical microscope (Renishaw microscope, equipped with 5×, 20×, 50×, and 100× short and long working distance microscope objectives) used to focus the excitation light and collect it in a backscattering configuration, a monochromator, notch filters system, and a charge coupled detector. The sample is mounted on a translation stage of a Leica microscope. The excitation used consists of a diode laser at 532 nm. The system has been calibrated against the 520.5 cm^{-1} line of an internal silicon wafer. The spectra have been registered in the 60−300 cm^{-1} range, particularly sensitive to the Pb−I modes. The final data have been averaged over a hundred accumulations in order

DOI: 10.1021/jacs.5b09085
J. Am. Chem. Soc. 2015, 137, 15451−15459

to maximize the signal-to-noise ratio. The measurements were conducted at room temperature and in air. The laser power intensity has been kept of the order of 300 μW in order to avoid any sample degradation effects.

■ ASSOCIATED CONTENT

Supporting Information

The Supporting Information is available free of charge on the ACS Publications website at DOI: 10.1021/jacs.5b09085.

Figures S1−S12 (PDF)

■ AUTHOR INFORMATION

Corresponding Authors

*E-mail annamaria.petrozza@iit.it (A.P.).
*E-mail srinivasa.srimath@iit.it (A.R.S.K.).

Present Address

S.D.S.: Research Laboratory of Electronics, Massachusetts Institute of Technology, 77 Massachusetts Avenue, Cambridge, MA 02139. G.G.: EPFL Valais Wallis EPFL SCI-SB-MN Rue de l'Industrie 17 Case postale 440 CH-1951 Sion.

Notes

The authors declare no competing financial interest.

■ ACKNOWLEDGMENTS

The authors acknowledge the funding from the EU Seventh Framework Progam [FP7/2007-203] under grant agreement number 604032 of the MESO project and DESTINY Marie-Curie network under grant agreement number 316494, and The Royal Society International Exchanges Scheme 2012/R2. The authors also thank Prof Guglielmo Lanzani for insightful discussions.

■ REFERENCES

(1) Kojima, A.; Teshima, K.; Shirai, Y.; Miyasaka, T. *J. Am. Chem. Soc.* **2009**, *131*, 6050−6051.
(2) Lee, M. M.; Teuscher, J.; Miyasaka, T.; Murakami, T. N.; Snaith, H. J. *Science* **2012**, *338*, 643−647.
(3) Kim, H. S.; Lee, C. R.; Im, J. H.; Lee, K. B.; Moehl, T.; Marchioro, A.; Moon, S. J.; Humphry-Baker, R.; Yum, J. H.; Moser, J. E.; Grätzel, M.; Park, N. G. *Sci. Rep.* **2012**, *2*, 591.
(4) Xing, G.; Mathews, N.; Sun, S.; Lim, S. S.; Lam, Y. M.; Grätzel, M.; Mhaisalkar, S.; Sum, T. C. *Science* **2013**, *342*, 344−347.
(5) Wehrenfennig, C.; Eperon, G. E.; Johnston, M. B.; Snaith, H. J.; Herz, L. M. *Adv. Mater.* **2014**, *26*, 1584−1589.
(6) Jeon, N. J.; Noh, J. H.; Kim, Y. C.; Yang, W. S.; Ryu, S.; Seok, S. Il. *Nat. Mater.* **2014**, *13*, 897−903.
(7) NREL Solar Cell Efficiency Chart.
(8) Tan, Z.-K.; Moghaddam, R. S.; Lai, M. L.; Docampo, P.; Higler, R.; Deschler, F.; Price, M.; Sadhanala, A.; Pazos, L. M.; Credgington, D.; Hanusch, F.; Bein, T.; Snaith, H. J.; Friend, R. H. *Nat. Nanotechnol.* **2014**, *9*, 687−692.
(9) Deschler, F.; Price, M.; Pathak, S.; Klintberg, L. E.; Jarausch, D.-D.; Higler, R.; Hüttner, S.; Leijtens, T.; Stranks, S. D.; Snaith, H. J.; Atatüre, M.; Phillips, R. T.; Friend, R. H. *J. Phys. Chem. Lett.* **2014**, *5*, 1421−1426.
(10) Xing, G.; Mathews, N.; Lim, S. S.; Yantara, N.; Liu, X.; Sabba, D.; Grätzel, M.; Mhaisalkar, S.; Sum, T. C. *Nat. Mater.* **2014**, *13*, 476−480.
(11) Zhu, H.; Fu, Y.; Meng, F.; Wu, X.; Gong, Z.; Ding, Q.; Gustafsson, M. V.; Trinh, M. T.; Jin, S.; Zhu, X.-Y. *Nat. Mater.* **2015**, *14*, 636−642.
(12) D'Innocenzo, V.; Grancini, G.; Alcocer, M. J. P.; Kandada, A. R. S.; Stranks, S. D.; Lee, M. M.; Lanzani, G.; Snaith, H. J.; Petrozza, A. *Nat. Commun.* **2014**, *5*, 3586.
(13) Even, J.; Pedesseau, L.; Katan, C. *J. Phys. Chem. C* **2014**, *118*, 11566−11572.
(14) Lin, Q.; Armin, A.; Nagiri, R. C. R.; Burn, P. L.; Meredith, P. *Nat. Photonics* **2014**, *9*, 106−112.
(15) Miyata, A.; Mitioglu, A.; Plochocka, P.; Portugall, O.; Wang, J. T.-W.; Stranks, S. D.; Snaith, H. J.; Nicholas, R. J. *Nat. Phys.* **2015**, *11*, 582−587.
(16) Saba, M.; Cadelano, M.; Marongiu, D.; Chen, F.; Sarritzu, V.; Sestu, N.; Figus, C.; Aresti, M.; Piras, R.; Geddo Lehmann, A.; Cannas, C.; Musinu, A.; Quochi, F.; Mura, A.; Bongiovanni, G. *Nat. Commun.* **2014**, *5*, 5049.
(17) Ponseca, C. S.; Savenije, T. J.; Abdellah, M. A.; Zheng, K.; Yartsev, A. P.; Pascher, T.; Harlang, T.; Chabera, P.; Pullerits, T.; Stepanov, A.; Wolf, J.-P.; Sundstrom, V. *J. Am. Chem. Soc.* **2014**, *136*, 5189−5192.
(18) Stranks, S. D.; Burlakov, V. M.; Leijtens, T.; Ball, J. M.; Goriely, A.; Snaith, H. J. *Phys. Rev. Appl.* **2014**, *2*, 034007.
(19) Frost, J. M.; Butler, K. T.; Brivio, F.; Hendon, C. H.; Van Schilfgaarde, M.; Walsh, A. *Nano Lett.* **2014**, *14*, 2584−2590.
(20) Frost, J. M.; Butler, K. T.; Walsh, A. *APL Mater.* **2014**, *2* (8), 081506.
(21) Liu, S.; Zheng, F.; Koocher, N. Z.; Takenaka, H.; Wang, F.; Rappe, A. M. *J. Phys. Chem. Lett.* **2015**, *6*, 693−699.
(22) Grancini, G.; Srimath Kandada, A. R.; Frost, J. M.; Barker, A. J.; De Bastiani, M.; Gandini, M.; Marras, S.; Lanzani, G.; Walsh, A.; Petrozza, A. *Nat. Photonics* **2015**, *9*, 695−701.
(23) Xiao, Z.; Yuan, Y.; Shao, Y.; Wang, Q.; Dong, Q.; Bi, C.; Sharma, P.; Gruverman, A.; Huang, J. *Nat. Mater.* **2014**, *14*, 193−198.
(24) Bertoluzzi, L.; Sanchez, R. S.; Liu, L.; Lee, J.-W.; Mas-Marza, E.; Han, H.; Park, N.-G.; Mora-Sero, I.; Bisquert, J. *Energy Environ. Sci.* **2015**, *8*, 910−915.
(25) Leijtens, T.; Hoke, E. T.; Grancini, G.; Slotcavage, D. J.; Eperon, G. E.; Ball, J. M.; De Bastiani, M.; Bowring, A. R.; Martino, N.; Wojciechowski, K.; Mcgehee, M. D.; Snaith, H. J.; Petrozza, A. *Adv. Energy Mater.* **2015**, *5*, 1500962.
(26) Snaith, H. J.; Abate, A.; Ball, J. M.; Eperon, G. E.; Leijtens, T.; Noel, N. K.; Stranks, S. D.; Wang, J. T.-W.; Wojciechowski, K.; Zhang, W. *J. Phys. Chem. Lett.* **2014**, *5*, 1511−1515.
(27) Tress, W.; Marinova, N.; Moehl, T.; Zakeeruddin, S. M.; Nazeeruddin, M. K.; Gratzel, M. *Energy Environ. Sci.* **2015**, *8*, 995−1004.
(28) De Bastiani, M.; Dell'Erba, G.; Gandini, M.; D'Innocenzo, V.; Neutzner, S.; Kandada, A. R. S.; Grancini, G.; Binda, M.; Prato, M.; Ball, J. M.; Caironi, M.; Petrozza, A. *Advanced Energy Materials* **2015**, DOI: 10.1002/aenm.201501453.
(29) Tao, C.; Neutzner, S.; Colella, L.; Marras, S.; Kandada, A. R. S.; Gandini, M.; De Bastiani, M.; Pace, G.; Manna, L.; Caironi, M.; Bertarelli, C.; Petrozza, A. *Energy Environ. Sci.* **2015**, *8*, 2365.
(30) Hoke, E. T.; Slotcavage, D. J.; Dohner, E. R.; Bowring, A. R.; Karunadasa, H. I.; McGehee, M. D. *Chem. Sci.* **2015**, *6*, 613−617.
(31) Fan, Z.; Xiao, J.; Sun, K.; Chen, L.; Hu, Y.; Ouyang, J.; Ong, K. P.; Zeng, K.; Wang, J. *J. Phys. Chem. Lett.* **2015**, *6*, 1155−1161.
(32) Leijtens, T.; Stranks, S. D.; Eperon, G. E.; Lindblad, R.; Johansson, E. M. J.; McPherson, I. J.; Rensmo, H.; Ball, J. M.; Lee, M. M.; Snaith, H. J. *ACS Nano* **2014**, *8*, 7147−7155.
(33) Yamada, Y.; Nakamura, T.; Endo, M.; Wakamiya, A.; Kanemitsu, Y. *J. Am. Chem. Soc.* **2014**, *136*, 11610−11613.
(34) Greenham, N. C.; Peng, X.; Alivisatos, A. P. *Phys. Rev. B: Condens. Matter Mater. Phys.* **1996**, *54*, 17628−17637.
(35) Mendez, E. E.; Bastard, G.; Chang, L. L.; Esaki, L.; Morkoc, H.; Fischer, R. *Phys. Rev. B: Condens. Matter Mater. Phys.* **1982**, *26*, 7101−7104.
(36) Morana, M.; Wegscheider, M.; Bonanni, A.; Kopidakis, N.; Shaheen, S.; Scharber, M.; Zhu, Z.; Waller, D.; Gaudiana, R.; Brabec, C. *Adv. Funct. Mater.* **2008**, *18*, 1757−1766.
(37) D'Innocenzo, V.; Srimath Kandada, A. R.; De Bastiani, M.; Gandini, M.; Petrozza, A. *J. Am. Chem. Soc.* **2014**, *136*, 17730−17733.

(38) Zhang, Y.; Liu, M.; Eperon, G. E.; Leijtens, T.; McMeekin, D. P.; Saliba, M.; Zhang, W.; De Bastiani, M.; Petrozza, A.; Herz, L.; Johnston, M. B.; Lin, H.; Snaith, H. *Mater. Horiz.* **2015**, *2*, 315−322.
(39) Yuan, Y.; Chae, J.; Shao, Y.; Wang, Q.; Xiao, Z.; Centrone, A.; Huang, J. *Adv. Energy Mater.* **2015**, *5*, 1500615.
(40) Wojciechowski, K.; Leijtens, T.; Spirova, S.; Schlueter, C.; Hoerantner, M.; Wang, J. T.-W.; Li, C.-Z.; Jen, A. K.-Y.; Lee, T.-L.; Snaith, H. J. *J. Phys. Chem. Lett.* **2015**, *6*, 2399−2405.
(41) Leijtens, T.; Eperon, G. E.; Noel, N. K.; Habisreutinger, S. N.; Petrozza, A.; Snaith, H. J. *Adv. Energy Mater.* **2015**, *5*, 1500963.
(42) Gottesman, R.; Gouda, L.; Kalanoor, B. S.; Haltzi, E.; Tirosh, S.; Rosh-Hodesh, E.; Tischler, Y.; Zaban, A.; Quarti, C.; Mosconi, E.; De Angelis, F. *J. Phys. Chem. Lett.* **2015**, *6*, 2332−2338.
(43) Wehrenfennig, C.; Liu, M.; Snaith, H. J.; Johnston, M. B.; Herz, L. M. *J. Phys. Chem. Lett.* **2014**, *5*, 1300−1306.
(44) Zhu, Z.-Y.; Podzorov, V. *J. Phys. Chem. Lett.* **2015**, *6*, 4758−4761.
(45) Quarti, C.; Grancini, G.; Mosconi, E.; Bruno, P.; Ball, J. M.; Lee, M. M.; Snaith, H. J.; Petrozza, A.; Angelis, F. De. *J. Phys. Chem. Lett.* **2014**, *5*, 279−284.
(46) Grancini, G.; Marras, S.; Prato, M.; Giannini, C.; Quarti, C.; De Angelis, F.; De Bastiani, M.; Eperon, G. E.; Snaith, H. J.; Manna, L.; Petrozza, A. *J. Phys. Chem. Lett.* **2014**, *5*, 3836−3842.
(47) Mosconi, E.; Quarti, C.; Ivanovska, T.; Ruani, G.; De Angelis, F. *Phys. Chem. Chem. Phys.* **2014**, *16*, 16137−16144.
(48) Mosconi, E.; Amat, A.; Nazeeruddin, M. K.; Grätzel, M.; De Angelis, F. *J. Phys. Chem. C* **2013**, *117*, 13902−13913.
(49) Leguy, A. M. A.; Frost, J. M.; McMahon, A. P.; Sakai, V. G.; Kockelmann, W.; Law, C.; Li, X.; Foglia, F.; Walsh, A.; O'Regan, B. C.; Nelson, J.; Cabral, J. T.; Barnes, P. R. F. *Nat. Commun.* **2015**, *6*, 7124.
(50) Deretzis, I.; Alberti, A.; Pellegrino, G.; Smecca, E.; Giannazzo, F.; Sakai, N.; Miyasaka, T.; La Magna, A. *Appl. Phys. Lett.* **2015**, *106*, 131904.
(51) Fong, D. D.; Stephenson, G. B.; Streiffer, S. K.; Eastman, J. A.; Auciello, O.; Fuoss, P. H.; Thompson, C. *Science* **2004**, *304*, 1650−1653.
(52) Liu, G.; Nan, C.-W. *J. Phys. D: Appl. Phys.* **2005**, *38*, 584−589.
(53) Gruverman, A.; Kholkin, A. *Rep. Prog. Phys.* **2006**, *69*, 2443−2474.

DOI: 10.1021/jacs.5b09085
J. Am. Chem. Soc. 2015, 137, 15451−15459